Richtmyer-Meshkov Instability and Gas-particle Interaction of Contoured Shock-tube Flows: a Numerical Study

Yi Liu

Abstract—**In this paper, computational fluid dynamics (CFD) is utilized to characterize a prototype biolistic delivery system, the biomedical device based on the contoured-shock-tube design (CST), with the aim at investigating shocks induced flow instabilities within the contoured shock tube. The shock/interface interactions, the growth of perturbation at an interface between two fluids of different density are interrogated. The key features of the gas dynamics and gas-particle interaction are discussed**

keywords— **Simulation, Shock wave, Particle, Interface, Supersonic, Richtmyer-Meshkov Instability**

I. INTRODUCTION

Advances in computational methodologies and supercomputer facilities available today enable us to investigate detailed physics/mechanism in a wide range of scientific fundamentals and engineering applications. Experience in developing a contoured shock-tube (CST) technology and knowledge recently gained in the material modelling and instability studies motivate the present numerical study.

A unique biomedical device has previously been developed for a needle-free powdered DNA/drug delivery. The principle is utilising a compressed helium gas to entrain micron-sized particles into a transonic shock-tube flow and accelerate them uniformly towards the skin target [1-4]. This technology provides a unique capability to effectively deliver micro-particle formulation of drugs to the human skin or mucosal tissue with a specially designed supersonic nozzle. Prototype devices have shown to be clinically effective, pain-free and applicable to a large number of macromolecular drugs such as insulin and vaccines.

Upon the actuation and rupture of membranes, the interface between two fluids of different densities (helium and air gases) subjected to an impulsive acceleration (i.e., shock wave) becomes unstable. This instability is known as the Richtmyer-Meshkov instability (RMI). After the initial impulsive acceleration, the flow develops a complex, vortex-driven motion eventually leading to turbulence.

Such instabilities are of great interest in wide research communities, such as, the inertial confinement fusion (ICF). The RMI, generated when a shock wave refracts through the pusher/fuel interface, plays an important role. It differs from the constant-acceleration Rayleigh-Taylor instability (RTI) by the impulsive nature of the energy input the flow. Perturbations on the interface grow in size and cause the materials to mix. As a consequence, the RMI degrades the ICF performance by reducing the heating of the gas during the implosion stage and by inhibiting the thermonuclear reaction after ignition. In the CST devices, by contrast, the RMI can be properly controlled to improve segregation and activation of aggregated particles. As observed in clinical trials, small drug particles intend to aggregate undesirably in the cassette over a shelf life, potentially cause damage. Fundamental understanding of the RMI is of great importance in both applications and equally many others.

The dynamics of a general flow driven by the RMI is rather complex. As a result, it is studied experimentally, analytically and computation through various test problems with relatively simple initial geometries [5-7]. Most results reported have concentrated on the instability of initially single-scale (sinusoidal) or multimode perturbation in straight or conical configurations. To further understanding of the fundamental mixing processes and instability mechanisms, the growth instabilities from random initial perturbations, where many different perturbations are presented, are investigated in a correctly-designed diverging supersonic nozzle of the CST configuration. The preliminary computational results have demonstrated the complexity of the CST flow field under the consideration.

In this study, CFD is employed to further investigate the performance of the CST system. A brief description of CST device is first given in Section II. Section III presents CFD methodology of choice. The gas flow is modeled and analyzed though a series of numerical calculations in Section IV. New insight into dynamics of the mixing processes and instability are explored. Effects of Atwood numbers (measurer of density difference between two fluids), locations of initial perturbations and shock strengths on the flow instability, material mixing and subsequent turbulent characteristics are investigated.

II. BIOLISTIC SYSTEM AND SUPERSONIC NOZZLES

A hand-held biolistic contoured shock tube (CST) system, configured for clinical uses, was developed. Key components of the shown device are a helium micro-cylinder, a drug

cassette and a conical nozzle (converging-diverging supersonic nozzle or contoured-shock-tube). The system with a contoured-shock-tube (CST) for accommodating the correctly-expended waves, instead of a converging-divergent supersonic nozzle of earlier biolistic delivery systems, is concerned in this paper. Prototype CST devices were studied [3, 4, 8].

In this study, we concentrate on computational fluid dynamics (CFD) simulations of the simplest CST configuration to better explain the experimental observations and gain a more thoroughly understanding of flow physics.

III. NUMERICALAL METHOD

A. Mathematical model and Numerical procedure

The two-dimensional, axisymmetric Navier-Stokes (NS) equations are

$$\frac{\partial U}{\partial t} + \frac{\partial F}{\partial x} = \frac{\partial G}{\partial y} + S = 0$$

where $U = [\rho, \rho u, \rho v, \rho E]^T$ is the independent vector with variables ρ, u, v and E denoting density, velocity components and specific total energy; F, G and S are the convective flux vectors and source term, respectively.

To accurately model the main features of the unsteady motion of the shock wave process, an efficient solver, the Modified Implicit Flux Vector Splitting (MIFVS) scheme is adapted [3]. It has been the establishment of an implicit difference scheme and eigenvalue analysis of the matrix for the Navier-Stokes equations. Compared to conventional implicit methods, the MIFVS is a Jacobian spectral radius scheme and a non-approximate-factorization scheme. Since matrix operation is not needed, the amount of computing work in each time step can be significantly reduced. It has been demonstrated that the current implicit formulation is adequately efficient when applied to FVS methods, while maintaining the high level of accuracy and robustness. For transient calculations, a dual time stepping was carried out to provide an efficient time-dependant solution of unsteady flows.

B. Initial/boundary conditions

Figure 1 displays computational domains for prototype devices, which is the simplest configuration for the CST system. The experimental results were reported [8]. The rupture pressure is 1550 kPa (determined from experimental measurement). The non-reflective boundary condition is specified at the far-field boundaries. The wall temperature is assumed to be constant during operation (less than 1 ms of interest for micro-particle delivery), with a non-slip condition.
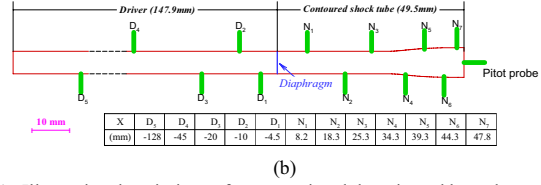

X (mm)	D₅	D₄	D₃	D₂	D₁	N₂	N₁	N₃	N₄	N₅	N₆

X (mm)	D₅	D₄	D₃	D₂	D₁	N₂	N₁	N₃	N₄	N₅	N₆
	-128	-45	-20	-10	-4.5	8.2	18.3	25.3	34.3	39.3	44.3	47.8

(b)

Fig. 1. Illustrative descriptions of computational domain and boundary conditions.

C. Computational grid

The computational domains are extended to $20D \times 10D$ (D, diameter of the shock tube) from the downstream of the nozzle exit. Both grids have 132,140 cells with 890 points along the axis direction and 129 points in the radial direction inside the CST domain. The remains are distributed downstream of the nozzle. The mesh is concentrated near the wall for a better numerical resolution.

CFD calculations with different grids are conducted for a grid-independency study. The most important parameters have been monitored on typical positions and no differences larger than 0.1% have been observed over a transient process of interest. Therefore, grid-independent solutions have reached in current transient supersonic flow studies.

IV. RESULTS AND DISCUSSION

A. Gas dynamics and code validation

We first present simulated pressure contour plots within the CST configuration with no initial interface perturbation imposed.

To validate the proposed computational method, we firstly compare calculated and measured pressure histories, with the locations shown in Figure 1. CFD simulations are also performed with commercial code, *Fluent*. The onset of diaphragm rupture is set as the time of zero. In Figures 2a, the pressure histories in the driver (P_1 and P_2) are plotted. An averaged value of 1550 kPa is assumed to be rupture pressure in the CFD calculations. In Figures 2b and 2c, the calculated pressure histories at locations P_2 and P_3, are compared with experiments measurements.
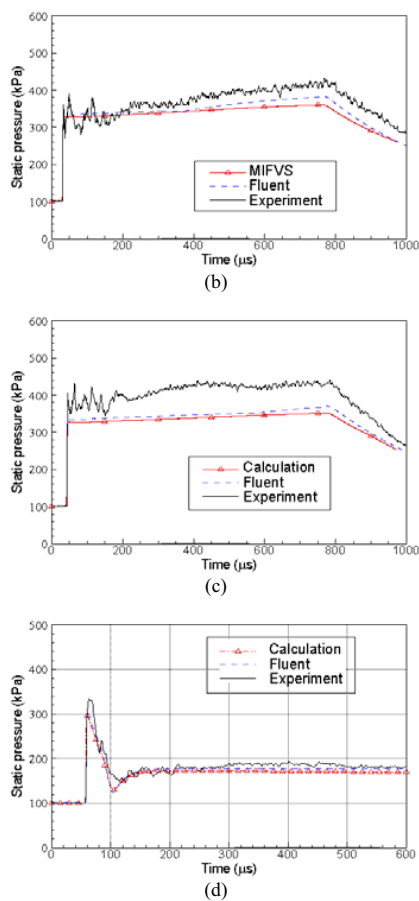

(a)

(b)

(c)

(d)
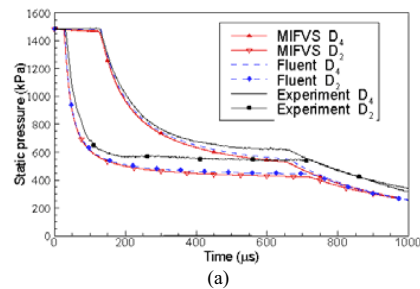
Fig. 2. Comparisons between calculated and measured pressure (a)-(e).

Figures 2d presents calculated and measured pressure traces at the location P_7, illustrating a typical starting process for a supersonic nozzle, respectively. The flow is initiated by a primary shock (indicated by the sudden pressure rise), which opens a transient starting process, followed by a quasi-steady supersonic flow region.
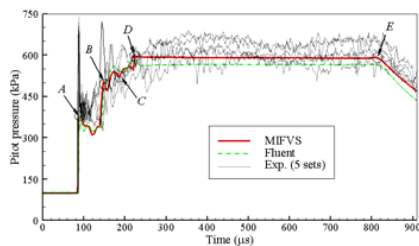

Fig. 3. Comparisons between calculated and measured pressure

Figure 3 compares the Pitot pressure histories among simulation and measurements. The experimental shot-to-shot variation in the Pitot probe is illustrated, with a sample of 5 shots. It will further illustrated in two-dimensional contour plots.

B. Gas-particle interaction

With simulated gas flow fields, it is possible to integrate gas-particle interactions. A comparison between the calculated, and measurements by the PIV system has been made in Figure 4. The action of the gas flow accelerating the particles was calculated with three different drag correlations ((Kurian and Das, 1997, Igra and Takayama, 1993, Henderson, 1976) within turbulent modelled flow field. One can see that the discrepancies between the calculated and the measured mean particle velocities at the nozzle exit were all within $\pm 10\%$. The simulation results show a good agreement with the experimental PIV image in terms of the particle velocity magnitude and locations.
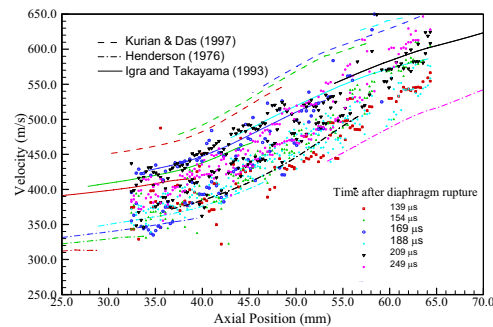

Fig. 4. Comparisons between calculated and experimental particle velocity at the centreline of the contoured shock tube section.

C. Single wavelength initial perturbation

Mixing induced by the propagation of shock waves nomal to the interface is now considered. A two-demensional simulation was carried out with the following initial amplitude perturbation at the interface:

$$\xi(y) = a_0 \cos\left(\frac{2\pi y}{Y}\right)$$

with a_0=0.12mm and Y=6 mm.

Figure 5 displays simulated time sequence of density contour plots, which indicates the flow features subject to shock wave impact within the constant area shock tube section. The perturbation is imposed by the presence of the sinusoidal interface. The density ratio, ρ_1 / ρ_2, at the interface remains in the region of 8-10.

In Figure 5a, initial contact surfaces and a heavier gas column are clearly sketched. Upon the rupture of the diaphragm, a primary shock wave is generated and propagates downstream towards the gas column, as shown in Figure 5b. The interaction between the shock and the sinusoidal interface induces the flow instability, identified in density contour plots (5c), (5d) and (5e). The growth of the initial amplitude perturbation at the interface is clear shown.
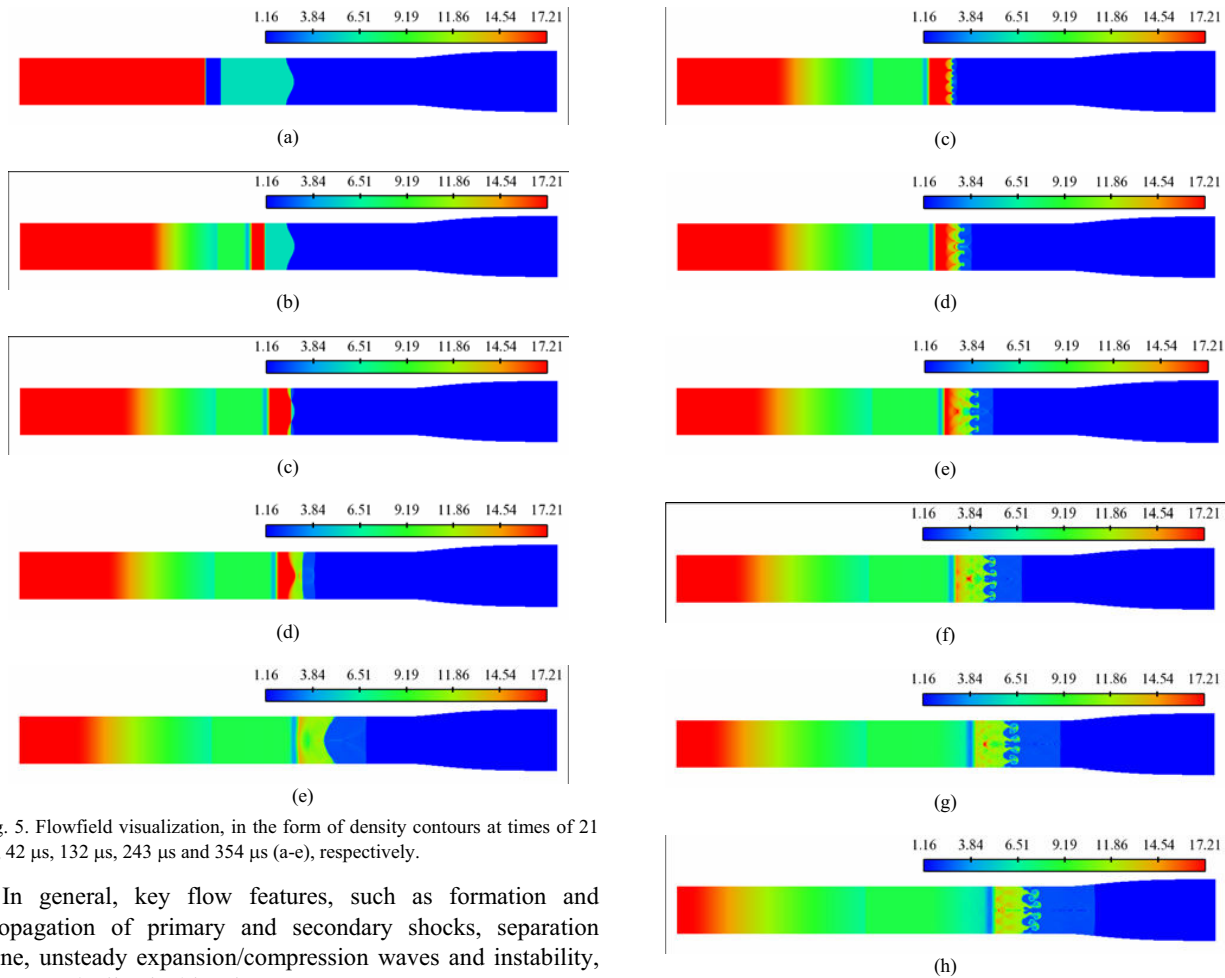
Fig. 5. Flowfield visualization, in the form of density contours at times of 21 µs, 42 µs, 132 µs, 243 µs and 354 µs (a-e), respectively.

In general, key flow features, such as formation and propagation of primary and secondary shocks, separation zone, unsteady expansion/compression waves and instability, are numerically elucidated.

D. Multi-wavelength initial interface perturbation

To further interrogate correctly expanded supersonic nozzle instability features subject to the propagation of shock waves, multi-wavelength amplitude perturbation is calculated.

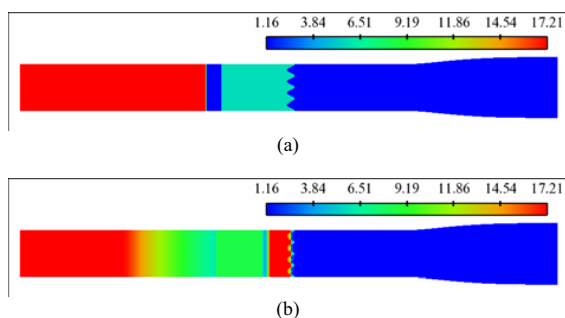Figure 5 plots simulated evolutions of the density contours, with flow pattern clear shown.

Fig. 5. Flowfield visualization, in the form of density contours at times of 21 µs, 42 µs, 132 µs, 243 µs and 354 µs (a-h), respectively.

These simulations and comparisons provide a valuable guideline for the design, optimization and evaluation of the drug delivery system.

V. CONCLUSIONS

Transient gas dynamics within a prototype biolistic device have been investigated numerically. A CFD approach has been implemented in order to gain new insights into the behavior of the contoured-shock-tube system (CST), configured for accelerating micro-particles to impact the outer layer of human skin. The new features of flow instability are explored.

Simulated pressure histories agree well with the corresponding reported static pressure measurements. These calculations have been used to further explore the gas flow field, with an emphasis on the nozzle starting process and RMI studies for the CST system.

The action of the gas flow accelerating the particles was

calculated with three different drag correlations within modeled flow fields. It was found that the discrepancies between the calculated and the measured mean particle velocities at the nozzle exit were all within $\pm$ 10%. Furthermore, the experiments and calculations both show that nominally uniform velocity has been achieve.

The utilization of RMI for initial particle segregation and its effects on the particle acceleration are currently investigated.

REFERENCES

[1] B.J. Bellhouse, D.F. Sarphie and J.C. Greenford (1994) Needless syringe using supersonic gas flow for micro-particle delivery, Int. Patent WO94/24263

[2] B.J. Bellhouse, N.J. Quinlan and R.W. Ainsworth (1997) Needle-less delivery of drugs, in dry powder form, using shock waves and supersonic gas flow, Proc. 21st Int. Symp. on Shock Waves, Queensland, Australia

[3] Y. Liu, and M.A.F. Kendall (2004) Numerical Simulation of Heat Transfer from a Transonic Jet Impinging on Skin for Needle-free Powdered Drug and Vaccine Delivery, Journal of Mechanical Engineering Science, Proceedings of the Institution of Mechanical Engineers Part C, 218(11): 1373-1383

[4] Y. Liu (2007) Impact studies of high speed micro-particles following biolistic delivery. IEEE Transactions on Biomedical Engineering 54(8): 1507-1513.

[5] D.L. Youngs (1994) Numerical simulation of mixing by Rayleigh-Taylor and Richtmyer-Meshkov instability, Laser Particle Beams 12(4): 725-750

[6] R.L. Holmes, G. Dimonte, B. Fryxell, M.L. Gittings, J.W. Grove, M. Schneider, D.H. Sharp, A.L. Velikovich, R.P. Weaver and Q. Zhang (1999) Richtmyer-Meshkov instability growth: experiment, simulation and theory, Journal of Fluid Mechanics 389: 55-79

[7] S. Kumar, P. Vorobieff, G. Orlicz, A. Palekar, C. Tomkins, C. Goodenough, M. Marr-Lyon, K.P. Prestridge and R.F. Benjamin (2007) Complex flow morphologies in shock-accelerated gaseous flows, Physica D: Nonlinear Phenomena, 235(1-2): 21-28

[8] N.K. Truong, Y. Liu, M.A.F. Kendall (2006) Gas and particle dynamics of a contoured shock tube for pre-clinical microparticle drug delivery, Shock Waves, 15(3-4): 149-164

[9] C.B. Henderson (1976) Drag coefficient of spheres in continuum and rarefied flows, AIAA J. 14(6): 707-708.

[10] O. Igra, K. Takayama (1993) Shock tube study of the drag coefficient of a sphere in a non-stationary flow, Proc R. Soc. Lond. A, 442: 231-247.

[11] J. Kurian, H.K. Das (1997) Studies of shock Wave Propagation in gas-particle mixtures, in: Proc. 21st Int. Symp. on Shock Waves, Great Keppel Island, Australia.